

OPEN

Ecological parameter reductions, environmental regimes, and characteristic process diagram of carbon dioxide fluxes in coastal salt marshes

Khandker S. Ishtiaq & Omar I. Abdul-Aziz

We investigated the ecological parameter reductions (termed “similitudes”) and characteristic patterns of the net uptake fluxes of carbon dioxide (CO₂) in coastal salt marshes using dimensional analysis method from fluid mechanics and hydraulic engineering. Data collected during May–October, 2013 from four salt marshes in Waquoit Bay and adjacent estuary, Massachusetts, USA were utilized to evaluate the theoretically-derived dimensionless flux and various ecological driver numbers. Two meaningful dimensionless groups were discovered as the light use efficiency number (LUE = CO₂ normalized by photosynthetically active radiation) and the biogeochemical number (combination of soil temperature, porewater salinity, and atmospheric pressure). A semi-logarithmic plot of the dimensionless numbers indicated the emergence of a characteristic diagram represented by three distinct LUE regimes (high, transitional, and low). The high regime corresponded to the most favorable (high temperature and low salinity) condition for CO₂ uptake, whereas the low regime represented an unfavorable condition (low temperature and high salinity). The analysis identified two environmental thresholds (soil temperature ~ 17 °C and salinity ~ 30 ppt), which dictated the regime transitions of CO₂ uptake. The process diagram and critical thresholds provide important insights into the CO₂ uptake potential of coastal wetlands in response to changes in key environmental drivers.

Coastal wetlands are among the most potent carbon sinks on earth, providing valuable ecosystem services such as global warming mitigation, storm protection, erosion control, and carbon sequestration^{1,2}. Understanding of the wetland carbon dioxide (CO₂) exchange processes is pivotal to the ecological stability because of the vulnerability of wetland ecosystems to global environmental change^{3,4}. The magnitude and variability of CO₂ in coastal wetlands depend on their complex nonlinear interplay with the major environmental drivers (e.g., light, temperature, salinity, pressure, and scales of measurements in time and space)^{5–7}. However, it remains unexplored whether the primary drivers of wetland CO₂ fluxes can be grouped into a reduced set of emergent generalizable entities that represent the coastal wetland productivity potentials in response to a changing environment. Therefore, a fundamental scientific question is whether we can identify ecological parametric reductions, known as “similitudes” in the domain of fluid mechanics and hydraulic engineering, describing environmental regimes of salt marsh CO₂ uptake. Do the salt marsh CO₂ fluxes represent any characteristic process path (e.g., diagram) with the covarying environmental drivers? Are there any critical environmental thresholds, indicating shifts in the process regimes of CO₂ fluxes? Answers to these scientific questions using similitude and dimensional analysis from fluid mechanics and hydraulic engineering may offer new insights into the underlying mechanistic principles and into the development of generalized predictive models of salt marsh CO₂ fluxes in space and time.

Wetlands are, in general, net sink of CO₂ during daytime due to photosynthesis and source during nighttime because of respiration⁸. There are multitudes of primary process drivers of salt marsh CO₂ exchanges with the atmosphere. Light is the main driver of net CO₂ uptake, whereas temperature mediates the photosynthesis process⁹. The temperature control on CO₂ uptake is intertwined with the activity of the primary photosynthesis enzyme, RuBisCO—which has a positive linkage with ambient temperature¹⁰. In contrast, salinity significantly

West Virginia University, P.O. Box 6103, Morgantown, WV 26506-6103, USA. ✉email: oiabdulaziz@mail.wvu.edu

reduces the CO₂ uptake rates and overall productivity in tidal wetlands by influencing the plants' physiological responses to available light^{11, 12}. Usually, salt marsh plants are resilient to high salinity; however, previous studies reported a considerable negative impact of salinity on the productivity of the salt marshes^{13, 14}. A high saline condition favors the accumulation of toxic hydrogen sulfide in anaerobic wetland soils—which adversely influences the salt marsh productivity¹⁵. Furthermore, high salinity reduces the nutrient uptake (e.g., nitrogen and phosphorous) of the marshes, and thereby decreases the productivity¹⁶.

Typically, salt marsh CO₂ uptake rates are higher during the high tides than the low tides, because salt accumulation during the low tides negatively impacts the productivity¹⁷. Abdul-Aziz et al.⁷ carried a comprehensive study to determine the major drivers of daytime CO₂ uptake in Waquoit Bay and adjacent estuaries, MA, USA using a systematic data analytics and empirical modeling approach. The study reported a substantially higher control and linkage of photosynthetically active radiation, soil temperature, and porewater salinity on instantaneous CO₂ uptake fluxes than that of pH, well water level, and soil moisture. Further, Abdul-Aziz et al.⁷ did not find any significant control of nitrogen loading gradient (5–126 kg/ha/year) on the CO₂ uptake fluxes across the study marshes; however, the authors reported significantly higher CO₂ uptake fluxes during high tides than the low tides.

A crucial advantage of identifying similitudes and dimensionless process groups is that information and underlying relationships and patterns can be generalized by utilizing data from different sites representing different gradients of response and predictor variables. In general, similitude represents the parametric reduction of a physical system by developing independent dimensionless groups or pi (Π) numbers, which functionally defines the mechanistic process of the system¹⁸. As the Π numbers represent different factors pertinent to the process, the fundamental description of the system defined by the associated process variables remains unchanged. Dimensional analysis using Buckingham pi-theorem is a useful method to decrease dimensions in data, reduce the number of parameters, and achieve similitude. The method is particularly useful in systems where simple governing equations cannot be used to represent the primary processes^{18, 19}.

Classical examples of similitudes and dimensional analysis that led to the development of generalized process diagrams and scaling relationships include “Moody diagram” in fluid mechanics and “Shields diagram” in sediment transport^{20, 21}. Here, the term “process diagram” refers to a graphical representation of different process states that a system follows in transition from one balanced condition to another. In “Moody Diagram”, seven original process variables of pipe flow were reduced to three process-based dimensionless groups using dimensional analysis, representing pipe friction and roughness across laminar, transitional, and turbulent flow regimes. Similarly, six process variables in rivers were used to formulate two meaningful dimensionless groups in “Shields diagram”, indicating different states of sediment transport across smooth, transitional, and rough flow regimes. Many studies in ecology, environmental sciences, and engineering utilized the concept of parametric reductions and dimensional analysis for process understanding and modeling^{22–30}. West et al.²² employed parametric reductions and scaling to derive a single universal curve to describe the growth rate of diverse species. Warnars et al.²⁴ applied dimensional analysis for parametric reductions in stream biogeochemistry, and developed useful scaling relationships between dimensionless biotic and abiotic factors in various streams across North America.

This study tests a fundamental hypothesis that the net CO₂ uptake fluxes in coastal salt marshes follow emergent ecological parameter reductions (i.e., similitudes) and distinct environmental regimes. The hypothesis was evaluated by formulating meaningful dimensionless numbers and defining different process regimes of salt marsh CO₂ uptake fluxes, leading to a characteristics process diagram. The field data collected from four salt marshes on the southern shore of Cape Cod, MA, USA were used to examine the hypothesis.

Materials and methods

Study wetlands and datasets. Four salt marshes located in Waquoit Bay and adjacent estuaries at Cape Cod, MA, USA were used as the case study sites: (1) Sage Lot Pond (SL), (2) Eel Pond (EP), (3) Great Pond (GP), and (4) Hamblin Pond (HP) (Fig. 1). The marshes represent a moderate gradient in nitrogen loading and a wide range of human population density^{31, 32}. On the basis of nitrogen loading influx, SL is in relatively pristine condition (~5 kg/ha/year), whereas HP (~29 kg/ha/year), EP (~63 kg/ha/year), and GP (~126 kg/ha/year) represent a medium to high nitrogen loading^{31, 33}. The vegetation community of the marshes is mostly dominated by *Spartina alterniflora* (a C₄ plant) in the low marsh zone.

A comprehensive detail on the collections and processing of gas fluxes and environmental variables for the four salt marshes were presented in Abdul-Aziz et al.⁷. Closed chamber-based measurements of the net ecosystem exchange (NEE) of CO₂ were made using a cavity ring-down spectrometer (CRDS) gas-analyzer (Model G2301, Picarro, Inc., Santa Clara, CA; frequency: 1 Hz; precision: 0.4 ppm) for different days during the extended growing season (May to October) in 2013 at the low marsh zones of the four salt marshes. The spectrometer analyzer was connected to the transparent, closed acrylic chamber (60 cm × 60 cm × 60 cm) through tubes. We calculated the molar concentrations of CO₂ in the chamber using the ideal gas law. The instantaneous molar concentrations of CO₂ were then linearly regressed with time (s). The regression slopes (i.e., rates of changes in CO₂ concentrations) were normalized by the chamber area (60 cm × 60 cm = 3,600 cm² = 0.36 m²) to compute the corresponding fluxes of CO₂ (i.e., changes in CO₂ concentrations per unit area and per unit time in μmol/m²/s) between the wetland soil and the atmosphere inside the chamber for each sampling period (typically ~5 min)^{6, 7}. To avoid impacts of any experimental error, a coefficient of determination (R²) of 0.90 was set as the minimum threshold for the regression to qualify the computed CO₂ fluxes as accurate and acceptable for analyses^{6, 7}.

The employed enclosed chamber-based technique of measuring CO₂ fluxes is a widely-used method in the carbon research domain^{34–37}. The technique provides an effective way to measure surface-atmospheric gas fluxes. As demonstrated above, the method first involves the calculation of the gradient of molar concentrations of CO₂ in time, which is then divided by the chamber area to compute the vertical CO₂ fluxes. Since the measurement

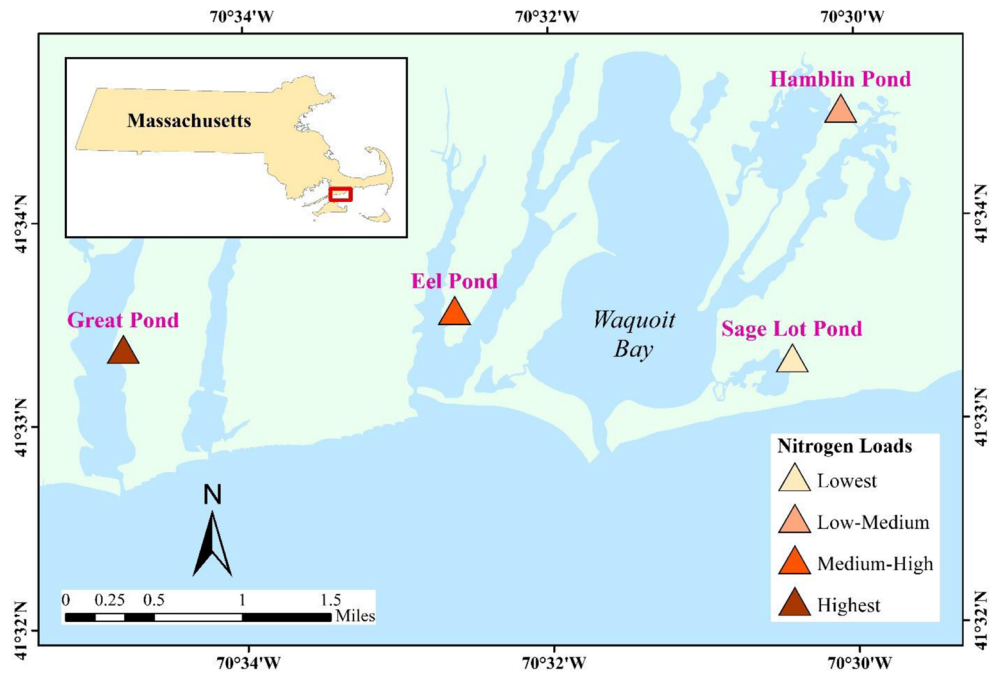


Figure 1. Locations of the case study salt marshes along the southern shore of Cape Cod in the Waquoit Bay and adjacent estuaries, MA. Nitrogen loading rates of the Sage Lot Pond, Hamblin Pond, Eel Pond, and Great Pond were 5, 29, 63, and 126 kg/ha/year, respectively.

chamber is small (e.g., 60 cm × 60 cm × 60 cm for our equipment) and enclosed, the vertical fluxes of CO₂ between soil and atmosphere (and not the divergence of CO₂ fluxes) drives the changes in CO₂ concentrations with time inside the chamber. Therefore, the chamber area-normalized rates of changes in CO₂ molar concentrations represent the vertical CO₂ gas fluxes between the soil and atmosphere inside the chamber.

The associated instantaneous environmental variables such as the photosynthetically active radiation (PAR), air temperature (AT), soil temperature (ST), and porewater salinity (SS) were concurrently measured⁷. The corresponding observations of atmospheric pressure (P_a) were collected from the nearby NOAA National Estuarine Research Reserve System (NOAA-NERRS) monitoring station located at Carriage House, MA³⁸. The filtered daytime net uptake fluxes of CO₂ ($NEE_{CO_2,uptake}$) represented the measurements made between 8 a.m. and 4.30 p.m. (Eastern Standard Time, EST), with the corresponding PAR higher than 1.5 $\mu\text{mole}/\text{m}^2/\text{s}$. AT was used to calculate the fluxes of $NEE_{CO_2,uptake}$ using the ideal gas law⁷; AT was, therefore, excluded as an environmental driver from further analyses. Instead, soil temperature (ST) was considered to represent the impact of temperature on $NEE_{CO_2,uptake}$. The dataset included 137 observational panels from the four study wetlands for 25 sampling days (Table S1, Figure S1 and S2 in Supplemental notes).

Theoretical formulation of dimensionless numbers through parametric reductions. Dimensional analysis using Buckingham pi (Π) theorem were applied to formulate wetland ecological similitudes and derive dimensionless functional groups or Π numbers^{18,20}. According to the pi theorem, a combination of n dimensional variables would lead to $(n - r)$ dimensionless Π numbers (r = number of relevant fundamental dimensions). $NEE_{CO_2,uptake}$, PAR, ST, SS, P_a , and the time-scale of measurement or estimation (t) were used for the dimensional analysis. PAR, ST, SS were the most dominant drivers of $NEE_{CO_2,uptake}$, as identified in the study of Abdul-Aziz et al.⁷. Furthermore, P_a negatively correlates with net photosynthesis as stomatal conductance increases with decreasing pressure³⁹. The selected variables for the dimensional analysis included four fundamental dimensions (mass: M; length: L; temperature: K; time: T) (Table 1). Since the variables were in different unitary systems, they were converted to the SI units by using appropriate conversion factors (Table 1). As the temperature dimension (K) was only represented by ST, specific heat of wet soil ($c_p = 1.48 \text{ kJ}/\text{kg}/\text{K}$) was further incorporated in the dimensional analysis to normalize ST. Following the pi theorem, a functional relationship (f) among the response ($NEE_{CO_2,uptake}$) and the potential predictors was expressed as follows:

$$f(NEE_{CO_2,uptake}, PAR, ST, SS, P_a, c_p, t) = 0 \quad (1)$$

where the total number of variables, $n = 7$; number of fundamental dimensions, $r = 4$. Therefore, the total number of possible Π numbers = $n - r = 3$. The functional relation of Eq. (1) was then represented with Φ in terms of dimensionless numbers as follows:

$$\Phi(\Pi_1, \Pi_2, \Pi_3) = 0 \quad (2)$$

Variables	Original units (X)	Converted units (Y)	Units conversation equation	Dimensions
NEE _{CO₂,uptake}	μmol/m ² /s	μmol/m ² /s	Y = X	[ML ⁻² T ⁻¹]
PAR	μmol/m ² /s	μmol/m ² /s	Y = X	[ML ⁻² T ⁻¹]
ST	°C	K	Y = 273.15 + X	[K]
SS	ppt	g/m ³	Y = 1,000 * X	[ML ⁻³]
P _a	millibar	g/m/s ²	Y = 100,000 * X	[ML ⁻¹ T ⁻²]
c _p = 1.48	kJ/kg/K	J/g/K	Y = X	[L ² T ⁻² K ⁻¹]
Time (t)	s	s	Y = X	[T]

Table 1. List of variables, units and dimensions used for the dimensional analysis. NEE_{CO₂,uptake}, PAR, ST, SS, P_a, and c_p refer, respectively, to daytime net uptake fluxes of CO₂, photosynthetically active radiation, soil temperature, porewater salinity, atmospheric pressure, and specific heat of wet soil. ppt refers to parts per thousand.

Based on the pi theorem, four variables ($r = 4$) could be considered as “repeating variables” in each iteration to formulate a dimensionless number by involving any of the remaining variables. Although the repeating variables should include all relevant fundamental dimensions (M, L, K, and T in this study), they should not form a dimensionless number among themselves. For example, considering PAR, ST, SS, and t as the “repeating variables”, the first pi number (Π_1) was expressed as follows:

$$\Pi_1 = PAR^a \cdot ST^b \cdot SS^c \cdot t^d \cdot NEE_{CO_2,uptake} \quad (3)$$

where a , b , c , and d were exponents. For Π_1 to be dimensionless, the following equation was obtained using the principle of dimensional homogeneity (i.e., equal dimensions on both sides):

$$M^0 \cdot L^0 \cdot T^0 \cdot K^0 = \left(\frac{M}{L^2 T}\right)^a \cdot (K)^b \cdot \left(\frac{M}{L^3}\right)^c \cdot (T)^d \cdot \frac{M}{L^2 T} \quad (4)$$

Therefore,

$$M^0 \cdot L^0 \cdot T^0 \cdot K^0 = M^{a+c+1} \cdot L^{-2a-3c-2} \cdot T^{-a+d-1} \cdot K^b \quad (5)$$

Equating the exponents of M, L, K, and T on both sides, we obtained the following matrix–vector form:

$$\begin{bmatrix} 1 & 0 & 1 & 0 \\ -2 & 0 & -3 & 0 \\ -1 & 0 & 0 & 1 \\ 0 & 1 & 0 & 0 \end{bmatrix} \begin{bmatrix} a \\ b \\ c \\ d \end{bmatrix} = \begin{bmatrix} -1 \\ 2 \\ 1 \\ 0 \end{bmatrix} \quad (6)$$

The system of linear equations was algebraically solved to compute the exponents as: $a = -1$, $b = 0$, $c = 0$, and $d = 0$ (see Text S1 in Supplemental notes for detailed algebraic equations and solutions). Therefore, from Eq. (3), we obtained the first pi number as

$$\Pi_1 = \frac{NEE_{CO_2,uptake}}{PAR} \quad (7)$$

Similarly, the other two Π numbers were formulated as (see Text S1 in Supplemental notes)

$$\Pi_2 = \frac{SS \cdot P_a}{PAR^2} \quad (8)$$

$$\Pi_3 = \frac{ST \cdot c_p \cdot SS^2}{PAR^2} \quad (9)$$

The pi theorem also allowed the derivation of new Π numbers by combining any two (or more) original Π numbers through multiplication or division as follows:

$$\Pi_4 = \Pi_2 \times \Pi_3 = \frac{ST \cdot c_p \cdot SS^3 \cdot P_a}{PAR^4} \quad (10)$$

$$\Pi_5 = \frac{\Pi_3}{\Pi_2} = \frac{ST \cdot c_p \cdot SS}{P_a} \quad (11)$$

Thus, the functional relationship of Eq. (2) could be represented in any of the following forms:

$$\Phi(\Pi_1, \Pi_4) = 0 \quad (12)$$

$$\Phi(\Pi_1, \Pi_5) = 0 \quad (13)$$

Therefore, dimensional analysis reduced the 7 original variables to 2–3 dimensionless numbers. Recalling the definition of similitude from the physical domain^{18,20}, such parametric reductions for the daytime net uptake fluxes of CO₂ and the associated environmental drivers were termed as “wetland ecological similitudes” in this research. As apparent, Π_1 represented the dimensionless CO₂ flux number (i.e., response), whereas Π_2 to Π_5 represented the environmental driver numbers (i.e., predictors).

Various sets of dimensionless numbers were obtained by iteratively changing the “repeating variables” (Table S2; see Text S1 in Supplemental notes for full derivations). However, only the unique Π numbers were considered for further analysis with empirical data. For example, $\frac{SS \cdot ST \cdot c_p}{PAR^2}$ (iteration-1 or 4 in Table S2) and $\frac{SS \cdot \sqrt{ST \cdot c_p}}{PAR}$ (iteration-3) were considered non-unique Π numbers, because the latter could be obtained as a square root function of the former. Similarly, $\frac{P_a}{PAR \cdot \sqrt{ST \cdot c_p}}$ (iteration-3) could be obtained from a square root and inversion of $\frac{PAR^2 \cdot ST \cdot c_p}{P_a^2}$ (iteration-2 or 5), and were considered the same number. Based on the pi theorem, the response Π number (i.e., dimensionless CO₂ flux number) were expressed as a general function (ψ) of all unique dimensionless environmental numbers as follows:

$$\frac{NEE_{CO_2, uptake}}{PAR} = \psi \left[\left(\frac{SS \cdot P_a}{PAR^2} \right), \left(\frac{ST \cdot c_p \cdot SS^2}{PAR^2} \right), \left(\frac{ST \cdot c_p \cdot SS^3 \cdot P_a}{PAR^4} \right), \left(\frac{ST \cdot c_p \cdot SS}{P_a} \right), \left(\frac{PAR^2 \cdot ST \cdot c_p}{P_a^2} \right), \left(\frac{SS \cdot P_a^3}{PAR^4 \cdot ST \cdot c_p} \right) \right] \quad (14)$$

Empirical analysis to determine the linkages among the derived numbers. The multivariate method of principal component analysis (PCA) was applied to the observational dataset from the salt marshes of Waquoit Bay to identify the important environmental driver number(s) that had dominant linkage(s) with the response pi number⁴⁰. PCA can resolve multicollinearity (mutual correlations) among the environmental driver numbers in a multivariate space, identifying the relatively unbiased information on their individual linkages with the response^{40,41}. To incorporate any non-linearity in the data matrix, observed (i.e., calculated) values of all pi numbers were log₁₀-transformed, which were further standardized (centralized and scaled) as follows: $Z = (X - \bar{X})/s_X$; $X = \log_{10}$ -transformed pi number, \bar{X} = mean of X , and s_X = standard deviation of X .

Results

Based on the existing literature, $\frac{NEE_{CO_2, uptake}}{PAR}$ was termed the “light use efficiency” (LUE) number, which represented salt marsh CO₂ uptake relative to the available sunlight (PAR)^{42–44}. Overall, the first two principal components (PCs) explained 90% of total variance in the dataset when PCA was performed using all unique dimensionless numbers (Eq. 14). The loadings of various dimensionless numbers on the first two PCs were presented in a biplot (Fig. 2), which indicated their interrelations, relative orientations, and groupings with vector lines. The nearly collinear (180°) orientation between LUE and $\frac{ST \cdot c_p \cdot SS}{P_a}$ suggested a high linkage between them. Similarly, the approximate collinearity (0° or 180° orientations) of vector lines for the remaining five environmental driver pi numbers indicated their strong interrelationships. However, the nearly orthogonal (90°) orientations of LUE with these other environmental driver numbers indicated their lack of linkages with the CO₂ flux number. Therefore, $\frac{ST \cdot c_p \cdot SS}{P_a}$ was considered as the most important and independent environmental driver number for LUE. $\frac{ST \cdot SS \cdot c_p}{P_a}$ was, therefore, termed the “biogeochemical” (BGC) number. Overall, dimensional analysis and PCA together reduced seven original variables to only two dimensionless groups. Based on Eq. (14), the LUE number was then expressed as the sole function of the BGC number as follows:

$$\frac{NEE_{CO_2, uptake}}{PAR} = \psi \left[\frac{ST \cdot SS \cdot c_p}{P_a} \right] \quad (15)$$

The derived “ecological similitude” is, therefore, a fundamental contribution in the field of atmosphere-wetland CO₂ fluxes. The application and usefulness of Eq. (15) in determining the emergent characteristic pattern, process regimes, and underlying relationships were then tested using the collected dataset from the four salt marshes of Cape Cod, MA.

Semi-logarithmic plot of the dimensionless LUE group as a function of the dimensionless BGC group showed a collapse of observed data from the four salt marshes into a unique dimensionless curve—indicating an emergence of similitude-based characteristic process diagram (Fig. 3). Two distinct regimes were identified from the plot along with a transitional regime that links the two. The zone defined by the $BGC \leq 0.13$ and $LUE \geq 0.002$ represents the high LUE regime, whereas $LUE < 0.002$ zone represents the low LUE regime. The transitional LUE regime ($BGC > 0.13$ and $LUE \geq 0.002$) connects the high and low LUE regimes. One-way ANOVA was utilized to test the null hypothesis of no significant difference in LUE between the respective regimes. Based on the ANOVA, the LUE in the high LUE regime was significantly different from the LUE values representing transitional ($F_{1,103} = 32.70$, p value < 0.0001) or low ($F_{1,72} = 175.92$, p value < 0.0001) regime (Table S3). Similarly, LUE values representing the transitional regime differed significantly from the low LUE regime ($F_{1,93} = 48.15$, p value < 0.0001). Overall, the developed curve indicated that CO₂ uptake relative to light in coastal wetlands was characterized by the corresponding variability in temperature and salinity, and the interactions thereof. The shift

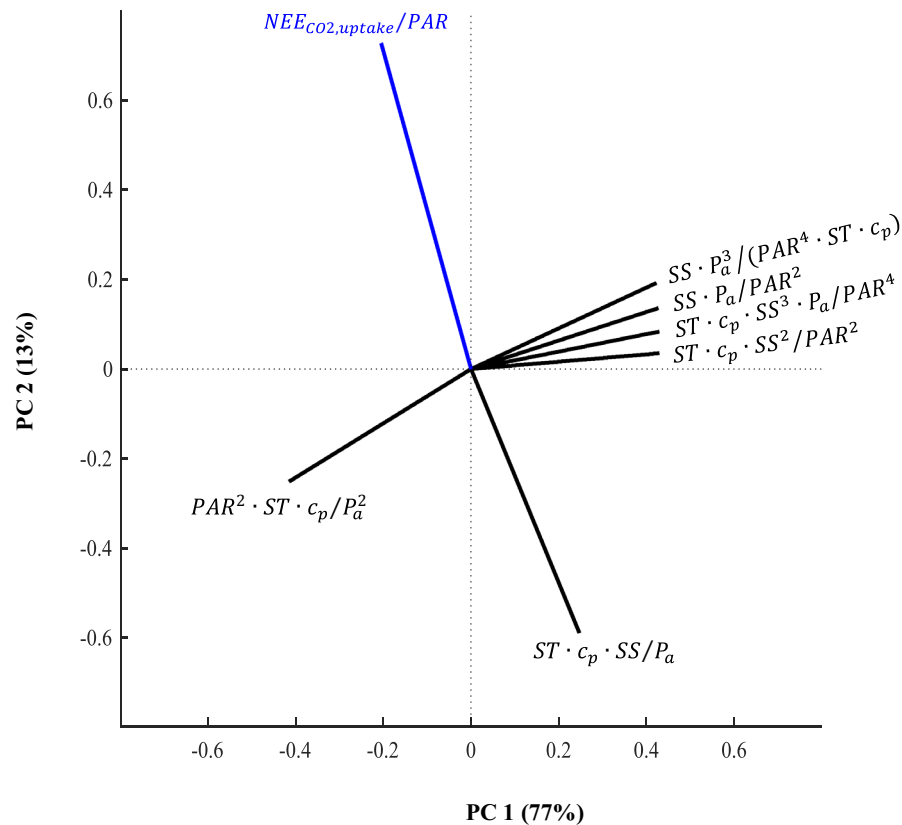


Figure 2. Biplots from principal component (PC) analysis, showing the interrelations, orientations, and groupings of the environmental driver dimensionless numbers with the response dimensionless number $\left(\frac{NEE_{CO_2,uptake}}{PAR}\right)$. $NEE_{CO_2,uptake}$, PAR, ST, SS, P_a , and c_p refer, respectively, to daytime net uptake fluxes of CO_2 , photosynthetically active radiation, soil temperature, porewater salinity, atmospheric pressure, and specific heat of wet soil.

from high to transitional regime was determined by the BGC value of 0.13 (Fig. 3). The CO_2 uptake efficiency had been consistently high for different reasonable combinations of ST and SS until $BGC = 0.13$ threshold was reached. The LUE, in general, decreased with increasing BGC when the curve crosses the 0.13 limit. However, once the curve had reached the hypothetical tipping point ($LUE = 0.0028$, $BGC = 0.145$), LUE dropped sharply with the decrease of BGC values—forming the multivalued-based “loop” shape of the curve.

The region of high LUE regime corresponded to the relatively high temperature ($ST \geq 17^\circ C$), and low to high salinity (10–30 ppt) (Table 2). The associated $NEE_{CO_2,uptake}$ and PAR varied within a wide range indicating their high variability, although the range of $\frac{NEE_{CO_2,uptake}}{PAR}$ was relatively narrow (approximately 0.003–0.01) (Fig. 3). In contrast, in the low LUE zone ($LUE < 0.002$), the range of temperature and salinity were relatively low ($\sim \leq 18^\circ C$) and high (29–38 ppt), respectively. Although adequate sunlight was available for photosynthesis in the low LUE regime (average $PAR = 1,130 \mu mol/m^2/s$)^{45, 46}, the CO_2 uptake (0.05–3 $\mu mol/m^2/s$; Table 2) and corresponding LUE (< 0.002) were considerably low. Similar to the low LUE regime, salinity was very high (30–40 ppt) in the transitional regime where the range of temperature was comparable to the high LUE regime. The corresponding $NEE_{CO_2,uptake}$ and PAR were higher in the transitional regime than the low LUE regime, but lower than the high LUE regime. Atmospheric pressure, P_a varied from 1,008 to 1,019 millibar in the high LUE regime; the ranges of P_a in the transitional and low LUE regimes were also comparable to the high LUE regime (Table 2).

Figure 3 and Table 2 suggested two critical environmental thresholds ($ST \sim 17^\circ C$ and $SS \sim 30$ ppt) that potentially defines the LUE regimes in coastal wetlands. Although the maximum temperature in the low LUE regime was $18^\circ C$ and minimum temperature in the transitional regime was $16^\circ C$, we chose their intermediate temperature ($ST \sim 17^\circ C$) as the threshold, which also represented the minimum temperature of the high LUE regime. Overall, the salt marsh CO_2 uptake followed the high regime when the temperature was approximately equal to or higher than $17^\circ C$ and salinity was lower or equal to 30 ppt (favorable condition for CO_2 uptake). In contrast, the low LUE regime was subject to low temperature and high salinity (unfavorable condition for CO_2 uptake) (Table 2). The transitional regime was mostly represented by high salinity stress ($SS \geq 30$ ppt) with relatively

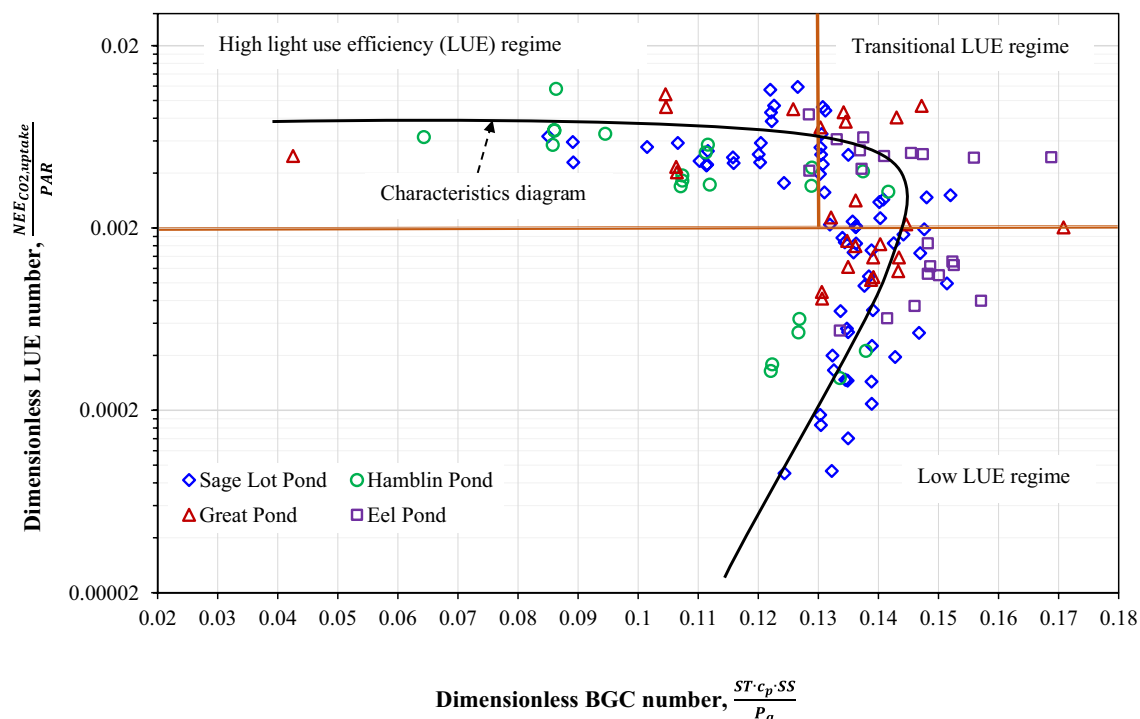


Figure 3. Plot of the dimensionless BGC number with the response dimensionless LUE number, revealing collapse of different variables on the generalized characteristics process diagram for wetland CO₂ fluxes. LUE refers to the dimensionless light use efficiency number ($\frac{NEE_{CO_2,uptake}}{PAR}$) and BGC refers to dimensionless biogeochemical number ($\frac{ST \cdot c_p \cdot SS}{P_a}$). NEE_{CO₂,uptake}, PAR, ST, SS, c_p, and P_a refer, respectively, to daytime net uptake fluxes of CO₂, photosynthetically active radiation, soil temperature, porewater salinity, specific heat of wet soil, and atmospheric pressure. The units of NEE_{CO₂,uptake} and PAR are in μmol/m²/s, ST is in Kelvin, SS is in g/m³, c_p is in J/g/K, and P_a is in g/m/s². The value of constant c_p = 1.48 J/g/K.

Variable	High LUE regime			Transitional LUE regime			Low LUE regime		
	Min	Max	Mean	Min	Max	Mean	Min	Max	Mean
NEE _{CO₂,uptake} (μmol/m ² /s)	5	17	10	2	17	7	0.05	3	1
PAR (μmol/m ² /s)	729	2,093	1,742	425	1,987	1,411	304	2,004	1,130
ST (°C)	17	26	21	16	26	20	9	18	14
SS (ppt)	10	30	25	30	40	33	29	38	33
P _a (millibar)	1,008	1,019	1,012	1,004	1,018	1,011	1,007	1,027	1,019

Table 2. Minimum (min), maximum (max) and mean of the daytime net uptake fluxes of CO₂ and the associated environmental variables for the high, transitional, and low LUE ($\frac{NEE_{CO_2,uptake}}{PAR}$) regimes, as shown in Fig. 3. NEE_{CO₂,uptake}, PAR, ST, SS, and P_a refer, respectively, to daytime net uptake fluxes of CO₂, photosynthetically active radiation, soil temperature, porewater salinity, and atmospheric pressure. LUE refers to light use efficiency.

favorable temperature (~ ≥ 16 °C) for photosynthesis—indicating a complex interplay between ST and SS in defining the transition from favorable uptake conditions to the unfavorable conditions.

Discussion

The functional convergence of LUE with the BGC number indicates the emergent parametric reductions of net CO₂ uptake fluxes in the *Spartina sp.* dominated salt marshes of Waquoit Bay and adjacent estuaries. Among the many definitions, LUE is conventionally defined as the net primary productivity (NPP) relative to the absorbed PAR^{42, 43}. However, instead of NPP to PAR ratio, we defined LUE as the ratio of NEE_{CO₂,uptake} to PAR in this paper. NEE_{CO₂,uptake} includes gross primary productivity, and autotrophic as well as heterotrophic respirations

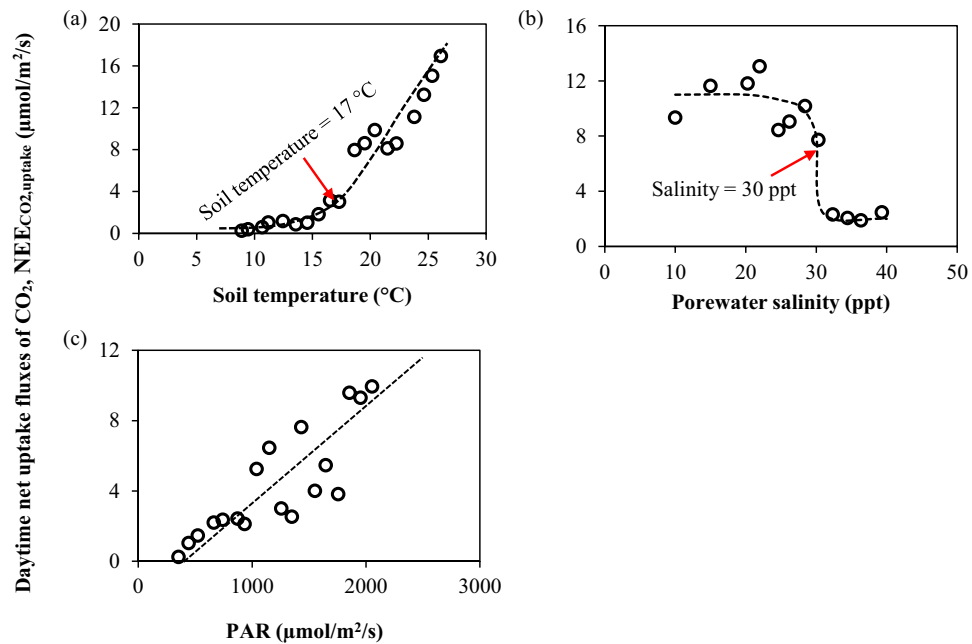


Figure 4. Plot of (a) soil temperature, (b) porewater salinity and (c) PAR with the corresponding $NEE_{CO_2,uptake}$ across the study marshes. The ST, SS, and PAR data were binned, respectively, for each 1 °C, 2 ppt, and 100 $\mu\text{mol}/\text{m}^2/\text{s}$ interval by pooling all the data across the four marshes. The bin averages of ST, SS, PAR and the corresponding average of $NEE_{CO_2,uptake}$ were then used to prepare the plot. The dotted line indicates the hypothetical trend line of $NEE_{CO_2,uptake}$ as a respective function of soil temperature, PAR or salinity. $NEE_{CO_2,uptake}$ refers to the daytime net uptake fluxes of CO_2 . PAR refers to the photosynthetically active radiation.

during daytime hours. There is not much research available on the LUE of wetland plants, particularly for salt marshes. Overall, C_4 plants such as *Spartina sp.* generally exhibit high photosynthetic efficiency relative to the C_3 species⁴⁷. For example, Jiang et al.⁴⁸ reported a higher light utilization by the *Spartina sp.* plants than the C_3 plants (*Phragmites australis* and *Scirpus mariqueter*) in the Yangtze River estuary, China. The comparatively higher LUE of C_4 plants stems from their ability to capture light for an extended growing period, higher uptake rates, and favorable physiology and biochemistry⁴⁹. Previous studies indicated a substantial influence of climatic, physiological, and biogeochemical factors (e.g., temperature, hydrology, canopy structure) on LUE for different species across ecosystems. Our study of the salt marsh CO_2 fluxes and the corresponding LUE corroborates the finding of existing literature that LUE is characteristically linked with the dynamics of the BGC number (Fig. 3).

The derived dimensionless BGC number represented the combined effect of temperature and salinity, and enveloped the effect within a narrow range (approximately 0.04–0.17). The impact of BGC group on the response LUE, which varied from approximately 0.000009 to 0.01, facilitated the identification of three underlying governing regimes (i.e., high, transitional, and low) and emergence of a characteristics process diagram of the salt marsh CO_2 fluxes. The identified soil temperature of ~ 17 °C and salinity of ~ 30 ppt thresholds dictated the transition of the CO_2 uptake efficiency from high to low regimes. However, such limiting thresholds were not apparent in case of P_a , although $NEE_{CO_2,uptake}$ can potentially decrease with increasing atmospheric pressure³⁹. Therefore, we hypothesized that variations of ST and SS were the major factors responsible for regime transition of CO_2 fluxes.

The identified 17 °C soil temperature threshold corresponds to the air temperature (AT) of 25.6 °C, which was obtained by developing a linear regression model of AT as a function of ST ($AT = 6.31 + 1.135 \times ST$; $R^2 = 0.61$) using the measured data from the four salt marshes. The estimated threshold of AT = 25.6 °C was comparable to the limiting air temperature threshold (20–25 °C) for photosynthesis¹⁰. Sage and Kubien¹⁰ also reported the role of photosynthesis enzyme, RuBisCo as a limiting factor on the CO_2 fixation of C_4 plants in a comparatively cool environment (i.e., AT < 20 °C). The turnover rate of RuBisCo generally increases with temperature during daytime hours, and the rate corresponds to the release of RuBP (ribulose-1, 5-bisphosphate) that facilitates the CO_2 fixation^{10,50}. Therefore, the low temperature in low LUE regime could represent the activation state of RuBisCo, where photosynthesis is extremely limited although the range of PAR in this regime was high enough to initiate a photosynthetic response (Table 2). The increase in CO_2 uptake with the soil temperature of 17 °C or higher was further apparent in Fig. 4a, where a jump in CO_2 uptake was observed at ST ~ 17 °C.

The most dynamic CO_2 uptake characteristic was observed in the transitional regime, which was separated from the high LUE regime based on the salinity threshold of 30 ppt. Because of the very high salinity ($SS \geq 30$ ppt), the uptake efficiency of the marshes decreased in the transitional regime, although the range of temperature in the transitional regime was comparable to the high LUE regime (Table 2). Previous studies reported a reduction of CO_2 assimilation rate in *Spartina sp.* marshes when salinity was higher than 30 ppt^{45,51,52}. High salinity significantly reduces the productivity by impacting the leaf chlorophyll content, protein synthesis, and

Study salt marshes	Sage lot pond	Hamblin pond	Great pond	Eel pond
NEE _{CO₂,uptake} (μmol/m ² /s)	5.5	6.9	4.5	4.1
PAR (μmol/m ² /s)	1,511.7	1,602.5	1,065.1	1,211.5
ST (°C)	17.5	18.7	17.2	17.1
SS (ppt)	31.0	26.0	31.0	34.0
P _a (millibar)	1,015.4	1,011.3	1,016.6	1,018.8
LUE (unitless)	0.004	0.004	0.004	0.003
BGC (unitless)	0.131	0.111	0.131	0.143
Operating LUE regime	Transitional	High	Transitional	Transitional

Table 3. Operating LUE regimes of the four study salt marshes using site-specific May–October, 2013 average values of NEE_{CO₂,uptake} and corresponding major drivers. The units of the variables were converted based on the conversion factors showed in Table 2 to compute the corresponding LUE and BGC numbers. The operating regimes for each of the ponds were determined by plugging in the computed BGC and LUE values in the developed characteristics diagram shown in Fig. 3. NEE_{CO₂,uptake}, PAR, ST, SS, and P_a refer, respectively, to daytime net uptake fluxes of CO₂, photosynthetically active radiation, soil temperature, porewater salinity, and atmospheric pressure. LUE refers to the dimensionless light use efficiency number $\left(\frac{NEE_{CO_2,uptake}}{PAR}\right)$ and BGC refers to dimensionless biogeochemical number $\left(\frac{ST \cdot c_p \cdot SS}{P_a}\right)$. ppt refers to parts per thousand. The value of constant specific heat of wet soil, $c_p = 1.48$ J/g/K.

lipid metabolism^{11, 53, 54}. Further, high salinity-driven osmotic stress could expedite the stomatal conductance, which substantially hinders the photosynthesis rate⁵⁵.

The observed reduction of CO₂ uptake above 30 ppt salinity was further revealed in Fig. 4b, which showed a reverse S-shaped curve of CO₂ fluxes in response to the changes in salinity from 10 to 40 ppt. The plot indicated an abrupt drop in NEE_{CO₂,uptake} when salinity reached 30 ppt; further, NEE_{CO₂,uptake} remained consistently low above the 30 ppt threshold. Therefore, we conjecture that temperature acts as a limiting factor to control the salt marsh CO₂ uptake in the low LUE regime when ST is approximately equal to or less than ~17 °C. However, once temperature crosses the limiting threshold and reaches a favorable condition, CO₂ uptake efficiency increases while salinity ~30 ppt emerges as a new limiting factor in controlling the LUE. It is worth mentioning here another limiting salinity threshold of 18 ppt above which the net CO₂ uptake in tidal marshes is remarkably greater than the methane (CH₄) emissions⁵⁶. Overall, the high LUE regime corresponds to the “most favorable” climatic-biogeochemical condition (high temperature and low salinity) of CO₂ uptake, whereas the low LUE regime corresponds to the “least favorable” condition (low temperature and high salinity) of CO₂ uptake. In contrast, the transitional regime represents relatively favorable climatic condition (relatively high temperature) but unfavorable biogeochemical condition (high salinity) for CO₂ uptake.

The CO₂ fixation efficiency in *Spartina sp.* marshes can also be low because of light saturation⁴⁵. However, NEE_{CO₂,uptake} was observed to have a linear increasing trend with PAR (Fig. 4c) in the salt marshes at Cape Cod, indicating no clear impacts of photo-inhibition or light saturation on the productivity during our sampling periods in May–October of 2013. Further, any reduction of LUE due to a lack of water availability (hydraulic limitation) was unlikely to occur for plants in these salt marshes, since the wetland soil remained mostly saturated due to the tidal inundations^{7, 57}.

The developed process diagram and insights into the governing regimes provide crucial information on the productivity and biogeochemical sensitivity of the coastal wetlands. Whether the salt marshes are efficiently assimilating CO₂ under ambient environmental conditions can be determined from Fig. 3. Salt marshes that consistently follow the low LUE regime would likely require intervention to make them more efficient. For example, any upward shift of a marsh from the low to transitional regime could potentially be achieved by reducing the salinity (i.e., decreasing BGC) with the enhancement of the freshwater inflow. However, ongoing wetland restoration practices involve augmentation of the tidal flow, which increases the salinity of the system and in turn inhibits CH₄ emission^{56, 58}. Therefore, our study highlights a need for a robust optimization in tidal flow control and salinity to make a balance between plants’ productivity and CH₄ emissions for an efficient system. Further, as high CO₂ uptake rate reduces the radiative forcing and contribute to global cooling⁵⁹, the identified regimes and characteristic diagram may be leveraged to map the potential coastal hotspots for radiative cooling.

Based on the process diagram (Fig. 3), the wetland managers can determine the operating regimes and rank the target wetlands in order of LUE. Although instantaneous fluxes and associated environmental variables were used to develop the diagram, the seasonal averages of the variables can be used to compute the corresponding BGC and LUE values. For example, by using the site-specific average values (May–October) of NEE_{CO₂,uptake} and the major drivers, the corresponding representative LUE and BGC numbers for the salt marshes were computed (Table 3). By plugging in the computed site-specific BGC and LUE values in Fig. 3, it was found that on average Sage Lot Pond, Great Pond and Eel Pond had been operating under the transitional LUE regime during the 2013 summer period. In contrast, the Hamblin Pond overall represented the high LUE regime. Comparatively lower mean salinity in the Hamblin Pond than the other ponds (Table 3, Figure S2) made the pond more efficient in CO₂ uptake relative to the available light. The results render these marshes strong candidates to be included in carbon crediting program as they are operating under transitional to high LUE regimes.

The analysis was conducted by using a single extended growing season data from four *Spartina sp.* dominated coastal salt marshes, although they represented a gradient in nitrogen loading in Waquoit Bay and adjacent estuaries. Data from other coastal wetlands across environmental and plant community gradients should be incorporated in future research to test the generalizability of the process diagram and critical thresholds for the net uptake fluxes of CO₂. Further, the presented parametric reductions and dimensional analysis method could be employed to develop similar process diagrams for other greenhouse gas (GHG) fluxes (e.g., CH₄). However, application of similitude and dimensional analysis requires a proper understanding of the underlying mechanisms and processes. Successful outcomes from the Buckingham pi theorem largely depend on an accurate selection of major processes and relevant variables. Involving too few or too many variables in the analysis would lead to misleading results. Further, the most meaningful outcomes (i.e., dimensionless groups) demand an exploration of all possible combinations of repeating and non-repeating variables in the analysis. However, once an appropriate and mechanistically meaningful set of dimensionless numbers such as LUE and BGC are identified through parametric reductions, these can indicate different environmental (lowly, transitional, and highly efficient) regimes of the targeted GHG fluxes. For example, the process diagram of CO₂ fluxes provided an overall understanding of the ecological health and carbon storage potential of the salt marshes in Cape Cod, MA. The information could be leveraged to spatially map coastal wetlands with a lower LUE (than 0.002; see Fig. 3) and higher BGC (than 0.13) to layout a detailed, but targeted sampling plan for restoration to a lower BGC and higher LUE. The research can, therefore, aid an efficient monitoring and management of coastal wetland carbon in a changing environment.

Conclusions

The study successfully tested the hypothesis that the net uptake fluxes of CO₂ in coastal salt marshes follow emergent ecological parameter reductions (similitudes) and distinct environmental regimes by using dimensional analysis. The research provided new insights into the first principles of wetland CO₂ processes. Two meaningful and important dimensionless numbers (“light use efficiency” and “biogeochemical”) were identified based on an application of the Buckingham pi theorem. A semi-logarithmic plot of the dimensionless numbers demonstrated the emergence of a process diagram, which was characterized by three governing light use efficiency (LUE) regimes (high, transitional, and low). Subject to the appropriate temperature and salinity conditions (soil temperature ≥ 17 °C and salinity ≤ 30 ppt) suitable for photosynthesis, the high LUE regime favors the most efficient utilization of available sunlight by wetland plants. In contrast, the CO₂ uptake rate relative to light was very low in the low LUE regime because of unfavorable ambient environmental conditions. Based on the characteristic process diagram, two critical environmental thresholds were identified (soil temperature ~ 17 °C and salinity ~ 30 ppt) to indicate regime transitions and wetland productivity.

The presented characteristic process diagram and environmental regimes would aid a targeted and efficient monitoring and management of tidal wetlands based on their CO₂ uptake efficiency. The temperature and salinity thresholds render valuable knowledge of salt marsh productivity and resiliency in response to changes in key environmental drivers. The study also highlights the importance of developing environmental regime-specific predictive models of CO₂ fluxes, compared to wetland-specific models, to minimize the site-specific model calibrations and uncertainty. The study can be considered a pioneering step in characterizing similitude-based emergent patterns and in identifying important process regimes of CO₂ and other GHG fluxes in coastal salt marshes.

Data availability

Data used in this study are described in main text, figures, tables, and Supplemental notes. The complete dataset is available in the figshare data repository at <https://doi.org/10.6084/m9.figshare.9856439>. The dataset is also available at <https://sites.google.com/view/ecological-water/data-and-models>.

Received: 22 January 2019; Accepted: 25 August 2020

Published online: 25 September 2020

References

1. Barbier, *et al.* The value of estuarine and coastal ecosystem services. *Ecol. Monogr.* **81**(2), 169–193 (2011).
2. Mcleod, *et al.* A blueprint for blue carbon: toward an improved understanding of the role of vegetated coastal habitats in sequestering CO₂. *Front. Ecol. Environ.* **9**(10), 552–560 (2011).
3. Kirwan, M. L. & Megonigal, J. P. Tidal wetland stability in the face of human impacts and sea-level rise. *Nature* **504**, 53–60 (2013).
4. Macreadie, *et al.* Can we manage coastal ecosystems to sequester more blue carbon?. *Front. Ecol. Environ.* **15**(4), 206–213 (2017).
5. Tokoro, *et al.* Net uptake of atmospheric CO₂ by coastal submerged aquatic vegetation. *Glob. Change Biol.* **20**(6), 1873–1884 (2014).
6. Moseman-Valtierra, *et al.* Carbon dioxide fluxes reflect plant zonation and belowground biomass in a coastal marsh. *Ecosphere* **7**(11), 1–21 (2016).
7. Abdul-Aziz, *et al.* Environmental controls, emergent scaling, and predictions of greenhouse gas (GHG) fluxes in coastal salt marshes. *J. Geophys. Res. Biogeosci.* **123**, 2234–2256 (2018).
8. Juszczak, R., Acosta, M. & Olejnik, J. Comparison of daytime and nighttime ecosystem respiration measured by the closed chamber technique on a temperate mire in Poland. *Pol. J. Environ. Stud.* **21**(3), 643–668 (2012).
9. Schäfer, K. V. R., Tripathee, R., Artigas, F., Morin, T. H. & Bohrer, G. Carbon dioxide fluxes of an urban tidal marsh in the Hudson-Raritan estuary. *J. Geophys. Res. Biogeosci.* **119**(11), 2065–2081 (2014).
10. Sage, R. F. & Kubien, D. S. The temperature response of C3 and C4 photosynthesis. *Plant Cell Environ.* **30**(9), 1086–1106 (2007).
11. Parida, A. K. & Das, A. B. Salt tolerance and salinity effects on plants: a review. *Ecotoxicol. Environ. Saf.* **60**(3), 324–349 (2005).
12. Callaway, J. C., ThomasParker, V., Vasey, M. C. & Schile, L. M. Emerging issues for the restoration of tidal marsh ecosystems in the context of predicted climate change. *Madroño* **54**(3), 234–248 (2007).
13. Vasquez, E. A., Glenn, E. P., Guntenspergen, G. R., Brown, J. J. & Nelson, S. G. Salt tolerance and osmotic adjustment of *Spartina alterniflora* (Poaceae) and the invasive M haplotype of *Phragmites australis* (Poaceae) along a salinity gradient. *Am. J. Bot.* **93**(12), 1784–1790 (2006).

14. Wang, H., Hsieh, Y. P., Harwell, M. A. & Huang, W. Modeling soil salinity distribution along topographic gradients in tidal salt marshes in Atlantic and Gulf coastal regions. *Ecol. Modell.* **201**(3), 429–439 (2007).
15. Lamers, *et al.* Sulfide as a soil phytotoxin—a review. *Front. Plant Sci.* <https://doi.org/10.3389/fpls.2013.00268> (2013).
16. Portnoy, J. W. Salt marsh diking and restoration: biogeochemical implications of altered wetland hydrology. *Environ. Manag.* **24**(1), 111–120 (1999).
17. Morris, J. T. *Effects of Sea Level Anomalies on Estuarine Processes. Estuarine Science: A Synthetic Approach to Research and Practice* 107–127 (Island Press, Washington, 2000).
18. Kundu, P. K. & Cohen, I. M. *Fluid Mechanics* 3rd edn. (Elsevier, Academic Press, 2004).
19. Gibbings, J. C. *Dimensional Analysis* (Springer, Berlin, 2011).
20. Finnemore, E. J. & Franzini, J. B. *Fluid Mechanics with Engineering Applications* 10th edn. (McGraw-Hill, New York, 2002).
21. Hager, W. H. Bed-load transport: advances up to 1945 and outlook into the future. *J. Hydraul. Res.* **56**(5), 596–607 (2018).
22. West, G. B., Brown, J. H. & Enquist, B. J. A general model for ontogenetic growth. *Nature* **413**, 628–631 (2001).
23. O'Connor, *et al.* Quantity–activity relationship of denitrifying bacteria and environmental scaling in streams of a forested watershed. *J. Geophys. Res. Biogeosci.* **111**, G04014 (2006).
24. Warnaars, T. A., Hondzo, M. & Power, M. E. Abiotic controls on periphyton accrual and metabolism in streams: scaling by dimensionless numbers. *Water Resour. Res.* **43**, W08425 (2007).
25. Hondzo, M. & Warnaars, T. A. Coupled effects of small-scale turbulence and phytoplankton biomass in a small stratified lake. *J. Environ. Eng.* **134**(12), 954–960 (2008).
26. Morris, M. W., Hondzo, M. & Power, M. E. Scaling *Glossosoma* (Trichoptera) density by abiotic variables in mountain streams. *J. N. Am. Benthol. Soc.* **30**(2), 493–506 (2011).
27. Harris, L. A. & Brush, M. J. Bridging the gap between empirical and mechanistic models of aquatic primary production with the metabolic theory of ecology: an example from estuarine ecosystems. *Ecol. Modell.* **233**, 83–89 (2012).
28. Zelenáková, M., Slezinger, M., Slys, D. & Purc, P. A model based on dimensional analysis for prediction of nitrogen and phosphorus concentrations at the river station Izkovce, Slovakia. *Hydrol. Earth Syst. Sci.* **17**(1), 201–209 (2013).
29. Guentzel, *et al.* Measurement and modeling of denitrification in sand-bed streams under various land uses. *J. Environ. Qual.* **43**(3), 1013–1023 (2014).
30. Schwefel, R., Hondzo, M., Wüest, A. & Bouffard, D. Scaling oxygen microprofiles at the sediment interface of deep stratified waters. *J. Geophys. Res. Lett.* **44**, 1340–1349. <https://doi.org/10.1002/2016GL072079> (2017).
31. Valiela, I., Geist, M., McClelland, J. & Tomasky, G. Nitrogen loading from watersheds to estuaries: verification of the Waquoit Bay nitrogen loading model. *Biogeochemistry* **49**(3), 277–293 (2000).
32. Kroeger, K. D., Cole, M. L. & Valiela, I. Groundwater-transported dissolved organic nitrogen exports from coastal watersheds. *Limnol. Oceanogr.* **51**(5), 2248–2261 (2006).
33. Cole, M. L., Kroeger, K. D., McClelland, J. W. & Valiela, I. Macrophytes as indicators of land-derived wastewater: application of $\delta^{15}\text{N}$ method in aquatic systems. *Water Resour. Res.* **41**, W01014. <https://doi.org/10.1029/2004WRR003269> (2005).
34. Livingston, G. P. & Hutchinson, G. L. Enclosure-based measurement of trace gas exchange: applications and sources of error. In *Biogenic Trace Gases: Measuring Emissions from Soil and Water* Vol. 2 (eds Matson, P. A. & Harris, R. C.) 14–51 (Blackwell Science Ltd, Oxford, 1995).
35. Gao, G. F. *et al.* Exotic *Spartina alterniflora* invasion increases CH_4 while reduces CO_2 emissions from mangrove wetland soils in southeastern China. *Sci. Rep.* **8**, 9243. <https://doi.org/10.1038/s41598-018-27625-5> (2018).
36. Obrador, B. *et al.* Dry habitats sustain high CO_2 emissions from temporary ponds across seasons. *Sci. Rep.* **8**, 3015. <https://doi.org/10.1038/s41598-018-20969-y> (2018).
37. Yuan, *et al.* Rapid growth in greenhouse gas emissions from the adoption of industrial-scale aquaculture. *Nat. Clim. Change* **9**(4), 318–322 (2019).
38. NOAA National Estuarine Research Reserve System (NOAA-NERRS). System-wide Monitoring Program. Data accessed from the NOAA NERRS Centralized Data Management Office. <https://www.nerrsdata.org/> (2018).
39. Takeishi, *et al.* Effects of elevated pressure on rate of photosynthesis during plant growth. *J. Biotechnol.* **168**(2), 135–141 (2013).
40. Jolliffe, I. T. Principal component analysis: a beginner's guide—II. Pitfalls, myths and extensions. *Weather* **48**(8), 246–253 (1993).
41. Ishitq, K. S. & Abdul-Aziz, O. I. Relative linkages of canopy-level CO_2 fluxes with the climatic and environmental variables for US deciduous forests. *Environ. Manag.* **55**(4), 943–960 (2015).
42. Medlyn, B. E. Physiological basis of the light use efficiency model. *Tree Physiol.* **18**(3), 167–176 (1998).
43. Yuan, *et al.* Global comparison of light use efficiency models for simulating terrestrial vegetation gross primary production based on the LaThuile database. *Agric. For. Meteorol.* **192**, 108–120 (2014).
44. Gitelson, A. A., Arkebauer, T. J. & Suyker, A. E. Convergence of daily light use efficiency in irrigated and rainfed C3 and C4 crops. *Remote Sens. Environ.* **217**, 30–37 (2018).
45. Kathilankal, *et al.* Physiological responses of *Spartina alterniflora* to varying environmental conditions in Virginia marshes. *Hydrobiologia* **669**, 167–181 (2011).
46. Long, S. P. & Woolhouse, H. W. The responses of net photosynthesis to light and temperature in *Spartina townsendii* (sensu lato), a C4 species from a cool temperate climate. *J. Exp. Bot.* **29**(4), 803–814 (1978).
47. Sage, R. F. The evolution of C4 photosynthesis. *New Phytol.* **161**(2), 341–370 (2004).
48. Jiang, L. F., Luo, Y. Q., Chen, J. K. & Li, B. Ecophysiological characteristics of invasive *Spartina alterniflora* and native species in salt marshes of Yangtze River estuary, China. *Estuar. Coast. Shelf Sci.* **81**(1), 74–82 (2009).
49. Zedler, J. B. & Kercher, S. Causes and consequences of invasive plants in wetlands: opportunities, opportunists, and outcomes. *Crit. Rev. Plant Sci.* **23**(5), 431–452 (2004).
50. Jensen, R. G. Activation of Rubisco regulates photosynthesis at high temperature and CO_2 . *Proc. Natl. Acad. Sci.* **97**(24), 12937–12938 (2000).
51. Percy, R. W. & Ustin, S. L. Effects of salinity on growth and photosynthesis of three California tidal marsh species. *Oecologia* **62**(1), 68–73 (1984).
52. Maricle, B. R. & Lee, R. W. Root respiration and oxygen flux in salt marsh grasses from different elevational zones. *Mar. Biol.* **151**(2), 413–423 (2007).
53. Mateos-Naranjo, *et al.* Synergic effect of salinity and CO_2 enrichment on growth and photosynthetic responses of the invasive cordgrass *Spartina densiflora*. *J. Exp. Bot.* **61**(6), 1643–1654 (2010).
54. Pierfelice, *et al.* Salinity influences on aboveground and belowground net primary productivity in tidal wetlands. *J. Hydrol. Eng.* **22**(1), D5015002 (2015).
55. Munns, R. & Tester, M. Mechanisms of salinity tolerance. *Annu. Rev. Plant Biol.* **59**, 651–681 (2008).
56. Poffenbarger, H. J., Needelman, B. A. & Megonigal, J. P. Salinity influence on methane emissions from tidal marshes. *Wetlands* **31**(5), 831–842 (2011).
57. Manzoni, *et al.* Hydraulic limits on maximum plant transpiration and the emergence of the safety–efficiency trade-off. *New Phytol.* **198**(1), 169–178 (2013).
58. Karberg, J. M., Beattie, K. C., O'Dell, D. I. & Omand, K. A. Tidal hydrology and salinity drives salt marsh vegetation restoration and *Phragmites australis* control in New England. *Wetlands* **38**(5), 993–1003 (2018).

59. Neubauer, S. C. & Megonigal, J. P. Moving beyond global warming potentials to quantify the climatic role of ecosystems. *Ecosystems* **18**(6), 1000–1013 (2015).

Acknowledgements

This research was funded by the U.S. National Science Foundation (NSF) (NSF CBET Environmental Sustainability Award Nos. 1705941 and 1561941/1336911) and by NOAA National Estuarine Research Reserve Science Collaborative (NA09NOS4190153), awarded to Omar I. Abdul-Aziz. We also thank Mohammed T. Zaki, a graduate research assistant working with Dr. Abdul-Aziz, for producing the study area map (Fig. 1) for this paper.

Author contributions

Both authors contributed to the writing of this manuscript. Abdul-Aziz generated the idea, derived the initial formulations, provided empirical evidence as proof of concept, and laid out the execution of the research as a part of his NSF proposal. Ishtiaq initially worked as a doctoral level research assistant and then as a post-doctoral fellow with Abdul-Aziz to arrive at the final formulations and results.

Competing interests

The authors declare no competing interests.

Additional information

Supplementary information is available for this paper at <https://doi.org/10.1038/s41598-020-72066-8>.

Correspondence and requests for materials should be addressed to O.I.A.-A.

Reprints and permissions information is available at www.nature.com/reprints.

Publisher's note Springer Nature remains neutral with regard to jurisdictional claims in published maps and institutional affiliations.



Open Access This article is licensed under a Creative Commons Attribution 4.0 International License, which permits use, sharing, adaptation, distribution and reproduction in any medium or format, as long as you give appropriate credit to the original author(s) and the source, provide a link to the Creative Commons licence, and indicate if changes were made. The images or other third party material in this article are included in the article's Creative Commons licence, unless indicated otherwise in a credit line to the material. If material is not included in the article's Creative Commons licence and your intended use is not permitted by statutory regulation or exceeds the permitted use, you will need to obtain permission directly from the copyright holder. To view a copy of this licence, visit <http://creativecommons.org/licenses/by/4.0/>.

© The Author(s) 2020